

Ca²⁺ Stores Regulate Ryanodine Receptor Ca²⁺ Release Channels via Luminal and Cytosolic Ca²⁺ Sites

Derek R. Laver

School of Biomedical Sciences, University of Newcastle and Hunter Medical Research Institute, Callaghan, New South Wales, Australia

ABSTRACT The free [Ca²⁺] in endoplasmic/sarcoplasmic reticulum Ca²⁺ stores regulates excitability of Ca²⁺ release by stimulating the Ca²⁺ release channels. Just how the stored Ca²⁺ regulates activation of these channels is still disputed. One proposal attributes luminal Ca²⁺-activation to luminal facing regulatory sites, whereas another envisages Ca²⁺ permeation to cytoplasmic sites. This study develops a unified model for luminal Ca²⁺ activation for single cardiac ryanodine receptors (RyR₂) and RyRs in coupled clusters in artificial lipid bilayers. It is shown that luminal regulation of RyR₂ involves three modes of action associated with Ca²⁺ sensors in different parts of the molecule; a luminal activation site (*L*-site, 60 μM affinity), a cytoplasmic activation site (*A*-site, 0.9 μM affinity), and a novel cytoplasmic inactivation site (*I*₂-site, 1.2 μM affinity). RyR activation by luminal Ca²⁺ is demonstrated to occur by a multistep process dubbed luminal-triggered Ca²⁺ feedthrough. Ca²⁺ binding to the *L*-site initiates brief openings (1 ms duration at 1–10 s⁻¹) allowing luminal Ca²⁺ to access the *A*-site, producing up to 30-fold prolongation of openings. The model explains a broad data set, reconciles previous conflicting observations and provides a foundation for understanding the action of pharmacological agents, RyR-associated proteins, and RyR₂ mutations on a range of Ca²⁺-mediated physiological and pathological processes.

INTRODUCTION

In cardiac muscle, contraction is mediated by depolarization and subsequent opening of voltage-dependent, L-type Ca²⁺ channels in the cell membrane (sarcolemma). Opening of these channels allows Ca²⁺ influx into the cell, which in turn opens Ca²⁺ release channels in the sarcoplasmic reticulum (SR) membrane. SR Ca²⁺ release can be a small highly localized increase in Ca²⁺ concentration called a spark, or can propagate along the cell in a Ca²⁺ wave, or can occur simultaneously along the length of the cell resulting in a global increase of Ca²⁺ called a transient (1). Ca²⁺ sparks are believed to be the elementary SR Ca²⁺ release event and Ca²⁺ waves and transients are thought to be the summation of spark events (2).

It has long been known that the excitability of Ca²⁺ release from muscle SR is substantially increased by its luminal Ca²⁺ load ([Ca²⁺]_L) (3,4). More recently, it has been shown that the excitability of neuronal endoplasmic reticulum (ER) is regulated in the same way, suggesting that modulation of Ca²⁺ signaling by [Ca²⁺]_L is a general phenomenon (5). However, the basis for load-dependent excitability remains controversial. Experiments on muscle cells and isolated SR vesicles have found that the effect of [Ca²⁺]_L on Ca²⁺ release could not be explained entirely by the associated Ca²⁺ gradient across the SR and that [Ca²⁺]_L must somehow control the Ca²⁺ permeability of the membrane (6,7). This was confirmed when activity of isolated RyRs in artificial bilayers was found to be modulated by [Ca²⁺]_L (8). At issue is the mechanism underlying the activation of RyRs by luminal Ca²⁺ being attributed to

two quite different processes. The true-luminal hypothesis attributes luminal Ca²⁺-activation and inhibition to Ca²⁺ regulatory sites on the luminal side of the RyR (9). The feedthrough hypothesis proposes that luminal Ca²⁺ permeates the pore and binds to cytoplasmic activation and inhibition sites (10–12). The latter is supported by the close correlation between the effect of [Ca²⁺]_L and Ca²⁺ flux (lumen to cytoplasm), and by the observation that luminal regulation is dependent on Ca²⁺ buffering on the cytoplasmic side of the membrane (11). However, there is an increasing body of evidence suggesting that there are sensing sites for Ca²⁺ regulation on the luminal side of the protein. For example, it has been shown that luminal Ca²⁺-activation is abolished by tryptic digestion of the luminal side of cardiac ryanodine receptors (RyR₂) (13). Although a recent bilayer study has presented evidence that both mechanisms somehow control skeletal ryanodine receptors (RyR₁) (14), it is not understood how cytoplasmic and luminal Ca²⁺ sites explain current observations or reconcile conflicting interpretations in the literature. In this study, measurements of the gating kinetics of isolated RyR₂ in lipid bilayers underlie the proposal of a novel mechanism for activation of RyRs by luminal-triggered Ca²⁺ feedthrough. This model predicts that in addition to cytoplasmic sites for Ca²⁺-activation and low affinity Ca²⁺/Mg²⁺-inhibition, RyRs possess a luminal Ca²⁺ binding site and a high affinity cytoplasmic Ca²⁺ inactivation site (Fig. 1). Ca²⁺ binding at the luminal site is sufficient to activate channel openings whereupon Ca²⁺ flows from lumen to cytoplasm (feedthrough) either enhances activation or causes inactivation.

Little is known about the mechanisms underlying the activation and termination of Ca²⁺ sparks in muscle. The quantal nature of Ca²⁺ spark intensities suggests that they

Submitted October 24, 2006, and accepted for publication January 22, 2007.

Address reprint requests to Dr. Derek Laver, Tel.: 61-2-4921-8732; E-mail: derek.laver@newcastle.edu.au.

© 2007 by the Biophysical Society

0006-3495/07/05/3541/15 \$2.00

doi: 10.1529/biophysj.106.099028

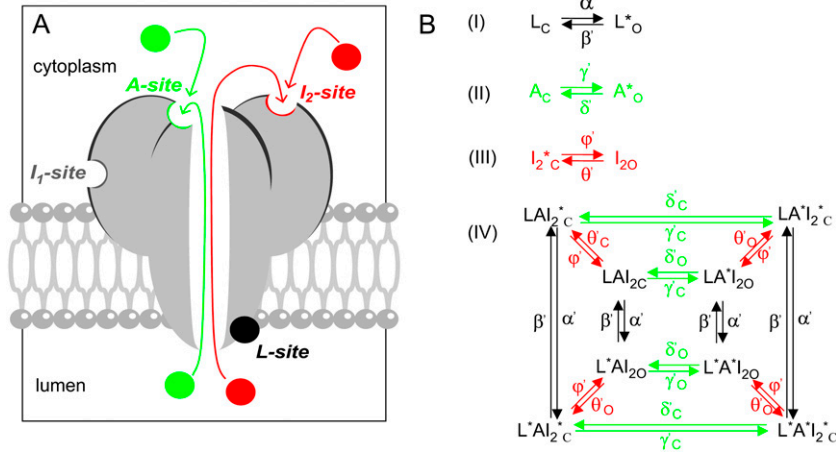


FIGURE 1 The luminal-triggered Ca^{2+} feedthrough model for $[\text{Ca}^{2+}]_L$ regulation of RyRs. (A) Schematic of luminal-triggered Ca^{2+} feedthrough. Ca^{2+} binding to the L -site causes channel opening whereupon luminal Ca^{2+} has access to the cytoplasmic Ca^{2+} activation (A -site) and inactivation sites (I_2 -site). The I_1 -site that mediates the low affinity $\text{Ca}^{2+}/\text{Mg}^{2+}$ is not included in the model (see text for details). (B) Kinetic schemes for Ca^{2+} binding at the L -, A -, and I_2 -sites (Schemes I–III) and the overall scheme (Scheme IV) resulting from the combined action of Ca^{2+} at all three sites. Schemes I–III are representations of multistep processes. Hence some reaction rates have complex dependencies on $[\text{Ca}^{2+}]$ and these are given in the equations listed in Table 1. Asterisks indicate sites occupied with Ca^{2+} . Reaction rates that depend on the Ca^{2+} current have subscripts o and c to indicate rates associated with open and closed channels, respectively. The open and closed status of the channel associated with each kinetic state is indicated by the subscripts O and C , respectively.

are produced by the concerted opening of up to 10 RyRs (15). Recent studies of the coupled gating of RyRs in artificial lipid bilayers may provide new insight into the triggering mechanisms for Ca^{2+} sparks (14,16,17). These investigations showed that Ca^{2+} feedthrough not only regulates the host RyR but also activates adjacent RyRs in a cluster. This study examines the roles of the luminal and cytoplasmic Ca^{2+} sites in generating this phenomenon in bilayers and how they might contribute to spark generation in muscle.

MATERIALS AND METHODS

SR vesicles (containing RyR₂) were obtained from sheep hearts and were reconstituted into artificial lipid bilayers as previously described (18). Lipid bilayers were formed from phosphatidylethanolamine and phosphatidylcholine (8:2 wt/wt) in *n*-decane (50 mg/ml). During experiments, the *cis* (cytoplasmic) and *trans* (luminal) solutions contained 250 mM Cs^+ (230 mM $\text{CsCH}_3\text{O}_3\text{S}$, 20 mM CsCl) and various concentrations of CaCl_2 . The *trans* solution was altered by addition of aliquots of stock solutions and the *cis* solution by local perfusion which allowed solution exchange within ~ 1 s (19).

Solutions were pH-buffered with 10 mM *n*-tris[Hydroxymethyl]methyl-2-aminoethanesulfonic acid and solutions were titrated to pH 7.4 using CsOH . Free $[\text{Ca}^{2+}]$ up to 100 nM was estimated using published association constants (20) and the program Bound and Determined (21) and concentrations higher than this were measured using a Ca^{2+} electrode (Radiometer, Copenhagen, Denmark). $[\text{Ca}^{2+}]$ below 10 μM was buffered with 4.5 mM 1,2-bis(*o*-aminophenoxy)ethane-*n,n,n',n'*-tetraacetic acid (4K^+) (BAPTA) and titrated with CaCl_2 . $[\text{Ca}^{2+}]$ in the range 10–50 μM was buffered with either sodium citrate (up to 6 mM) or dibromo BAPTA (up to 2 mM).

Acquisition and analysis of ion channel recordings

Bilayer apparatus and data recording methods have been described previously (14). Electrical potentials are expressed using standard physiological convention (i.e., cytoplasmic side relative to the luminal side at virtual ground). Measurements were carried out at $23 \pm 2^\circ\text{C}$. Before analysis, the current signal was digitally filtered at 1 kHz with a Gaussian

filter and sampled at 5 kHz. Single channel properties were measured using Channel2 software (P. W. Gage and M. Smith, Australian National University, Canberra). Open probability (P_o) and open and closed durations were calculated from single channel records using a threshold discriminator at 50% of channel amplitude. For experiments in which bilayers contained several RyRs, P_o was calculated from the time-averaged current divided by the unitary current and the number of channels (n). Both methods of calculating P_o gave similar results. The mean channel open and closed durations (τ_o and τ_c) could also be calculated from mean open and closed durations in multichannel recordings ($\tau_o(n)$ and $\tau_c(n)$), provided that multiple openings were rare: $\tau_o = \tau_o(n)$ and $\tau_c = \tau_c(n) \times n$. The number of channels in each experiment was determined during periods of strong activation, which were usually achieved by turning off the local perfusion and exposing the RyRs to the *cis* bath. The values τ_o and τ_c were calculated mainly from the recording of 100–1000 opening events. However, under conditions that produced extremely low channel activity, the mean durations were obtained from as few as 40 events covering >400 s of recording (sampling error $<40^{-1/2}$, i.e., $<16\%$). Dwell-time frequency histograms of channel open and closed events were obtained exclusively from single channel recordings and were displayed as probabilities (counts/total number of events). These were plotted using the log-bin method suggested by Sigworth and Sine (22), which displays exponentials as peaked distributions centered at their exponential time constant. Sampling bins were equally spaced on a log scale with 3.5 or 7 bins per decade.

On rare occasions ($<5\%$ of experiments), RyRs appeared to form coupled clusters in the bilayer, similar to that seen for RyR₁ (14). The experiments on coupled and uncoupled RyRs were analyzed and presented separately. Channel gating in coupled clusters was analyzed using the Hidden Markov Model (23), as described previously (14). The algorithm calculated the transition probability matrix of the underlying Markov process from the raw signal using maximum likelihood criteria. The mean channel opening and closing rates were calculated from the transition probability matrix.

Ca^{2+} -dependencies of P_o , τ_o , and opening rate were characterized by fitting these data with Hill curves using the following equations for activation and inactivation (shown here for the case of P_o , similar equations apply to τ_o and opening rate):

$$P_o = P_{\min} + \frac{(P_{\max} - P_{\min})([\text{Ca}^{2+}]/K_a)^{n_a}}{1 + ([\text{Ca}^{2+}]/K_a)^{n_a}},$$

$$P_o = P_{\min} + \frac{(P_{\max} - P_{\min})}{1 + ([\text{Ca}^{2+}]/K_i)^{n_i}}.$$

The expressions P_{\min} and P_{\max} are the activities of the minimally and maximally activated channel, K_a and K_i are the $[\text{Ca}^{2+}]$ for half-activation and inhibition, and n_a and n_i are the corresponding Hill coefficients. The theory was fitted with the data using the method of least-squares.

The luminal-triggered Ca^{2+} feedthrough model: Kinetic schemes and equations

RyRs are known to possess cytoplasmic sites for Ca^{2+} -activation (A -sites $\sim 1 \mu\text{M}$ affinity) and low-affinity $\text{Ca}^{2+}/\text{Mg}^{2+}$ -inhibition (I_1 -site, $\sim 10 \text{ mM}$ affinity, previously named the I -site). Based on novel data presented below, the model includes a cytoplasmic Ca^{2+} -inactivation site (the I_2 -site, which causes partial inactivation with $\sim 1 \mu\text{M}$ affinity) and a luminal activation site (L -site, $\sim 60 \mu\text{M}$ affinity). Fig. 1 *A* shows a schematic representation of the locations of these sites on the RyR protein. It is envisaged that the channel can open if Ca^{2+} is bound to either the A - or L -sites. Thus luminal Ca^{2+} can open the channel by binding to the L -site, whereupon the flow of Ca^{2+} through the pore can increase the cytoplasmic $[\text{Ca}^{2+}]$ in the vicinity of the pore mouth ($[\text{Ca}^{2+}]_p$) and reinforce channel activation (increasing τ_o) by binding to the A -site or inactivate the channel by binding to the I_2 -site (decreasing τ_o).

Kinetic schemes for Ca^{2+} binding at the L -, A -, and I_2 -sites are shown in Fig. 1 *B* (*I–III*) and the overall regulation of RyRs by the three Ca^{2+} sites is described by an eight-state model (Scheme *IV*) presenting the amalgamation of Schemes *I–III*. The equations describing the action of luminal and cytoplasmic Ca^{2+} on channel activity and the model parameters are listed in Table 1. The I_1 -site was not considered in the model calculations because Ca^{2+} feedthrough is unlikely to increase $[\text{Ca}^{2+}]_p$ to levels where significant Ca^{2+} binding will occur at this site.

The first step in developing the luminal-triggered Ca^{2+} feedthrough model was to formulate a phenomenological description of RyR₂ regulation by cytoplasmic Ca^{2+} . The kinetic schemes used previously to describe cytoplasmic Ca^{2+} -activation of RyRs are complex and involve many closed and open states (24,25). To avoid this level of complexity the whole cytoplasmic Ca^{2+} -activation process was lumped into two single-step Ca^{2+} binding schemes associated with the A - and I_2 -sites (Schemes *II* and *III* in Fig. 1 *B*). Thus, the parameters γ , δ , θ , ϕ , Δ , and K_i in Eqs. 4–10 were adjusted until the model fitted the cytoplasmic Ca^{2+} concentration ($[\text{Ca}^{2+}]_c$)-dependencies of τ_o and τ_c (Figs. 5 and 10). The second step was to ascertain the gating properties associated with the L -site (Scheme *I*). This was done by fitting the voltage/luminal Ca^{2+} concentration ($[\text{Ca}^{2+}]_p$)-dependence of τ_c (Fig. 6) using the parameters α , β , K_L in Eqs. 2 and 3. The final step was to calculate the effects of Ca^{2+} feedthrough on the voltage/ $[\text{Ca}^{2+}]_p$ -depen-

dencies of τ_o , τ_c , and their associated dwell-time distributions from theoretical estimates of $[\text{Ca}^{2+}]_p$ and compare these estimates with the data.

Ion diffusion theory (26) was used to calculate $[\text{Ca}^{2+}]_p$ and its dependence on I_{Ca} (pA) and distance from the pore (r , nm) under the buffering conditions used here.

$$[\text{Ca}^{2+}]_p = I_{\text{Ca}} \frac{825}{r} \exp\left(\frac{-r}{6}\right) + [\text{Ca}^{2+}]_c. \quad (1)$$

For a given distance from the pore, $[\text{Ca}^{2+}]_p$ has a linear dependence on I_{Ca} , which is encapsulated in the parameters X in Eq. 7b and Y in Eq. 10b (see Table 1). I_{Ca} was calculated using a rate theory model of RyR conductance (27). This part of the model has only two adjustable parameters, X and Y .

Model predictions were made by simulating the time series of channel gating events and using these to generate theoretical open and closed dwell time distributions, τ_o , τ_c , and P_o . For each set of experimental conditions, the model reaction rates were calculated using the equations in Table 1. The sojourn of the simulated channel through its various states was driven by a random number generator in conjunction with the transition probability matrix that was derived from the model reaction rates. Sequential open and closed events were marked by transitions between open and closed states in the model. The effects of limited time resolution in the data were accommodated by amalgamating simulated events shorter than $<200 \mu\text{s}$.

RESULTS

The effects of cytoplasmic and luminal Ca^{2+} on RyR₂ in the presence of ATP are presented here first because 1), it is recognized that the effects of luminal Ca^{2+} require the presence of cytoplasmic agonists such as ATP, caffeine, or sulmazole (8,28,29); and 2), ATP is the physiological coagonist. Data are presented that define the affinity and gating properties of one luminal and two cytoplasmic Ca^{2+} sites on RyR₂. These properties were used to construct the luminal-triggered Ca^{2+} feedthrough model. The results were then fitted by adjusting the model parameters associated with the proximity of the two cytoplasmic Ca^{2+} binding sites to the pore mouth. The model is then applied to elucidating the effects of ATP and ion channel coupling on RyR regulation by Ca^{2+} .

TABLE 1 Equations and parameters of the luminal-triggered Ca^{2+} feedthrough model

Eq.	Eq.					
<i>L</i>-site						
2	$\alpha' = \alpha \times \exp\left(\frac{\Delta eV}{kT}\right) \frac{[\text{Ca}^{2+}]_p^2}{K_L^2 + [\text{Ca}^{2+}]_p^2}$	3	$\beta' = \beta$	Affinity	Opening (0V)	V-dependence
				+ATP $K_L = 60 \mu\text{M}$	$\alpha = 2.7 \text{ s}^{-1}$	$\Delta = 0.4$
				-ATP $K_L = 45 \mu\text{M}$	$\alpha = 0.6 \text{ s}^{-1}$	$\Delta = 0.4$
						Closing
						$\beta = 1000 \text{ s}^{-1}$
						$\beta = 1000 \text{ s}^{-1}$
<i>A</i>-site						
4	$\gamma'_c = \gamma [\text{Ca}^{2+}]_c^3$	5	$\delta'_c = \delta [\text{Ca}^{2+}]_c^{-n}$	Affinity	Opening	Feedthrough
				+ATP $K_A = 1 \mu\text{M}$	$\gamma = 43 \text{ s}^{-1} \mu\text{M}^{-3}$	$X = 15 \mu\text{M/pA}$
6	$\gamma'_o = \gamma [\text{Ca}^{2+}]_p^3$	7a,	$\delta'_o = \delta [\text{Ca}^{2+}]_p^{-n}$	-ATP $K_A = 6 \mu\text{M}$	$\gamma = 1.0 \text{ s}^{-1} \mu\text{M}^{-3}$	$X = 15 \mu\text{M/pA}$
		7b	$[\text{Ca}^{2+}]_p = XI_{\text{Ca}} + [\text{Ca}^{2+}]_c$			$\delta = 220 \text{ s}^{-1} \mu\text{M} (n = 1)$
						$\delta = 700 \text{ s}^{-1} (n = 0)$
<i>I</i>₂-site						
8	$\theta'_c = \theta \frac{[\text{Ca}^{2+}]_c^2}{K_i^2 + [\text{Ca}^{2+}]_c^2}$	9	$\phi' = \phi$	Affinity	Closing	Feedthrough
				+ATP $K_i = 1.2 \mu\text{M}$	$\theta = 250 \text{ s}^{-1}$	$Y = 0.35 \mu\text{M/pA}$
10a	$\theta'_o = \theta \frac{[\text{Ca}^{2+}]_p^2}{K_i^2 + [\text{Ca}^{2+}]_p^2}$	10b	$[\text{Ca}^{2+}]_p = YI_{\text{Ca}} + [\text{Ca}^{2+}]_c$	-ATP $K_i = 1.2 \mu\text{M}$	$\theta = 800 \text{ s}^{-1}$	$Y = 0.35 \mu\text{M/pA}$
						Opening
						$\phi = 300 \text{ s}^{-1}$
						$\phi = 400 \text{ s}^{-1}$

Equations describe the $[\text{Ca}^{2+}]$ -dependencies of opening and closing rates associated with each site (refer to Scheme *IV* in Fig. 1 *B*). K_A was derived from the theoretical half-maximal $[\text{Ca}^{2+}]_c$ -activation of P_o and was not used in the fitting of the model. The reaction rates are distinguished from model parameters with an apostrophe (e.g., α'). γ' , δ' , and θ' depend on the Ca^{2+} current through the pore and therefore take on different values for the open and closed states (indicated by subscripts, o and c). In Eq. 2, T is the temperature in degrees K, k is the Boltzmann constant and V is bilayer voltage.

Activation of RyR₂ by cytoplasmic Ca²⁺ in the presence of ATP

It is shown that the activity of RyR₂ was dependent on both [Ca²⁺]_C (Fig. 2 A) and [Ca²⁺]_L (Fig. 2 B). The experiments in this section focus on the properties of the A- and I₂-sites as revealed by the effects of [Ca²⁺]_C on RyR₂ activity. Fig. 2 A highlights the gradual transition in the gating properties that occurs as the dominant cytoplasmic agonist switches from ATP to Ca²⁺. RyRs activated by ATP (100 nM [Ca²⁺]_C, Fig. 2 A, top three traces) had relatively long open and closed events compared to RyRs activated by high [Ca²⁺]_C (with 2 mM ATP, Fig. 2 A, bottom two traces). To probe the gating mechanisms for this behavior, RyR gating was analyzed by compiling frequency histograms of open and closed times. These could be described by the sum of two exponential decays (these appear as peaked distributions when using the log-bin method in Fig. 3). The time-constants and relative weighting of the exponential components depended on [Ca²⁺]_C and [Ca²⁺]_L. Time-constants within each open time distribution had a 3–10-fold separation and lay within the range 1–50 ms (e.g., dashed lines in Fig. 3 A). The closed time distributions varied considerably with [Ca²⁺]_C. In the presence of 0.1 μM [Ca²⁺]_C, two widely separated exponentials were clearly resolved (open arrows in Fig. 3 B) in which >80% of the events were associated with the longer time-constant. Raising [Ca²⁺]_C progressively reduced the longer time constant until both were quite similar at 10 μM (solid arrows in Fig. 3 B). The dwell-time distributions are frequently represented here by their means. The value τ_o gave a good representation of the average time-constant of the open time distribution and the value for τ_c lay within 20% of the longer closed time constant.

The effects of [Ca²⁺]_C on the RyR₂ gating properties, P_o, τ_o, and τ_c, are shown in Fig. 4. Cytoplasmic Ca²⁺ activated RyR₂ at μM levels (Fig. 4 A). Luminal Ca²⁺ had a marked effect on P_{min} at -40 mV (Hill parameters are listed in Table 2), whereas it had a relatively small effect on P_{max}. The values for K_a and hence A-site affinity, showed no significant dependence on [Ca²⁺]_L or membrane potential (P > 0.06, see Table 2). The [Ca²⁺]_C-dependencies of τ_o shown in Fig.

4 B reveal activation and inactivation processes associated with μM [Ca²⁺]_C. In the virtual absence of luminal Ca²⁺ ([Ca²⁺]_L < 10 μM), τ_o increased with [Ca²⁺]_C (channel activation, Fig. 4 B, solid circle), whereas 100 μM [Ca²⁺]_L unmasked a previously unidentified [Ca²⁺]_C-dependent inactivation that decreased τ_o (Fig. 4 B, open circle). Despite this inactivation, raised [Ca²⁺]_C caused an increase in P_o via a decrease in τ_c that overwhelmed the effect of inactivation (P_o = τ_o/(τ_c + τ_o) with τ_c ∝ [Ca²⁺]_C⁻³ in Fig. 4 C and τ_o ∝ [Ca²⁺]_C in Fig. 4 B). The value τ_o at 1000 μM [Ca²⁺]_L had values between those at <10 and 100 μM [Ca²⁺]_L and did not show a significant dependence on [Ca²⁺]_C. The value τ_c at 1000 μM [Ca²⁺]_L was very similar to that seen at 100 μM. The underlying mechanism for the complex effects of [Ca²⁺]_C and [Ca²⁺]_L on τ_o and τ_c are explained with the description of the model characteristics (see below).

In the model, the activation and inactivation phenomena are attributed to the A- and I₂-sites, respectively. The properties of these sites are derived from the data in Fig. 4 as follows: RyR gating due to the A-site is described by Scheme II (Fig. 1 B). In the absence of luminal Ca²⁺, the opening and closing rates associated with the A-site are reflected in the channel open and closed times (γ' ≈ 1/τ_c and δ' ≈ 1/τ_o). To account for the [Ca²⁺]_C-dependencies of τ_o and τ_c in Fig. 4, δ' ∝ [Ca²⁺]_C (Fig. 4 B, solid circle, Eqs. 5 and 7) and γ' ∝ [Ca²⁺]_C³ (Fig. 4 C, solid circle; Eqs. 4 and 6). RyR gating due to the I₂ inactivation site is described by Scheme III (Fig. 1 B) where the equivalent opening and closing rates (φ' and θ') are given by Eqs. 8–10a. Inactivation in response to [Ca²⁺]_C appears to be only partial (i.e., <40%), because even at 10 μM Ca²⁺ where the I₂-site is saturated, P_o > 0.6. To account for this the closing rate, θ', is given a sublinear dependence on [Ca²⁺]_P with an upper limit.

Bell-shaped dependence of RyR₂ activity on [Ca²⁺]_L in the presence of ATP

Although several studies have reported a bell-shaped [Ca²⁺]_L-dependence of RyR₁ P_o in the presence of ATP, there has

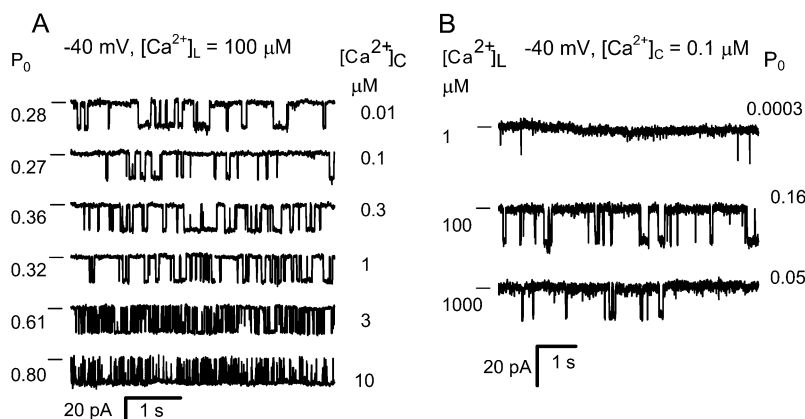


FIGURE 2 The effects of [Ca²⁺]_L and [Ca²⁺]_C on the activity of RyR₂ (-40 mV). (A) The effect of [Ca²⁺]_C on the activity of a RyR in the presence of 100 μM [Ca²⁺]_L. Increasing [Ca²⁺]_C increases P_o in association with a decrease in duration of mean open and closed events. Channel openings are downward current jumps from the baseline (indicated with a dash). (B) The effect of [Ca²⁺]_L on RyR activity in the presence of 0.1 μM [Ca²⁺]_C and 2 mM ATP.

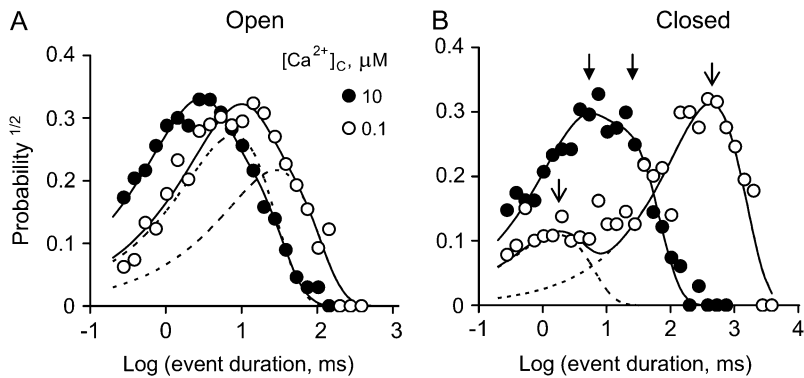


FIGURE 3 Dwell-time probability distributions of channel open (A) and closed (B) events. The data are plotted using the log-bin method of Sigworth and Sine (22). Event duration distributions were compiled from a single RyR, which was activated by 2 mM ATP and the indicated $[Ca^{2+}]_C$ in the presence of 100 $\mu M [Ca^{2+}]_L$ (-40 mV). An increase in $[Ca^{2+}]_C$ from 0.1 to 10 μM shifted both the open and closed distributions to shorter times. Solid curves show double-exponential fits to the data and dashed curves show individual exponential components for the fits to the open circles. When using the log-bin method the exponential components within these distributions appear as peaks centered at their respective time-constants. The arrows in panel B show the time constants associated with the data at 0.1 $\mu M [Ca^{2+}]_C$ (○, *open arrows*) and 10 $\mu M [Ca^{2+}]_C$ (●, *solid arrows*).

been no equivalent demonstration of this in RyR₂. In the absence of luminal Ca^{2+} the activity of RyR₂ was virtually zero ($P_o = (8 \pm 4) \times 10^{-4}$ at $[Ca^{2+}]_L \sim 0.1 \mu M$, $n = 6$) indicating a near-absolute requirement for luminal Ca^{2+} . Increasing $[Ca^{2+}]_L$ (from 1 to 100 μM at -40 mV) substantially increased the activity of the RyRs, whereas a further increase to 1 mM decreased channel activity (Fig. 2 B). At -60 mV and -40 mV, voltages favoring the flow of Ca^{2+} from luminal to cytoplasmic baths, the $[Ca^{2+}]_L$ for half-activation of P_o , was 50 μM (K_a for the *left side* of the *bell*) and $[Ca^{2+}]_L$ for half-inactivation was 1 mM (K_i for the *right side* of the *bell*, Fig. 5, A and B). Both K_a and K_i increased as the bilayer voltage became more positive (Fig. 5, C and D), and at positive voltages the decline in P_o was beyond the experimental range of $[Ca^{2+}]_L$ (K_i could no longer be monitored).

Luminal Ca^{2+} would not be expected to influence the channel-opening rate ($1/\tau_o$) other than by affecting a luminal site because cytoplasmic sites are inaccessible to luminal ions when the channel is closed. Therefore, analysis of τ_o and τ_c should provide valuable information of the effect of Ca^{2+} feedthrough in channel activation. The results show that $[Ca^{2+}]_L$ had very different effects on τ_o and channel

opening rate (Fig. 6). The value τ_o had a bell-shaped dependence on $[Ca^{2+}]_L$, which is shown at several voltages in Fig. 6 A (the bell is most clearly seen at -20 mV). The K_a and K_i values for the $[Ca^{2+}]_L$ -dependence of τ_o over the entire experimental voltage range is shown in Fig. 6 C. The values K_a and K_i increased with voltage in a way expected for Ca^{2+} ions, which must cross the membrane to reach their effector site (*long-dashed line*, Fig. 6 C). These results indicate that luminal Ca^{2+} activation and inactivation of τ_o are mediated by cytoplasmic facing sites. Moreover, the nonadditive effects of luminal and cytoplasmic Ca^{2+} on channel activation and inhibition indicate that the luminal and cytoplasmic actions are mediated by common binding sites.

Luminal Ca^{2+} activated RyR₂ by increasing their opening rate and approached a maximum (V_{max}) at high concentrations (Fig. 6 B). The voltage-dependence of K_a and V_{max} are shown in Fig. 6 D. The K_a indicates the involvement of a Ca^{2+} binding site with an affinity (K_L) $\sim 60 \mu M$ and the V_{max} indicates that the Ca^{2+} -bound site can trigger channel openings at a rate of $1-10 s^{-1}$. The K_a for opening rate did not show a significant voltage-dependence ($P > 0.15$, *t*-test) indicating that luminal Ca^{2+} ions do not move through the *trans*-membrane electric field to reach the site. V_{max} varied

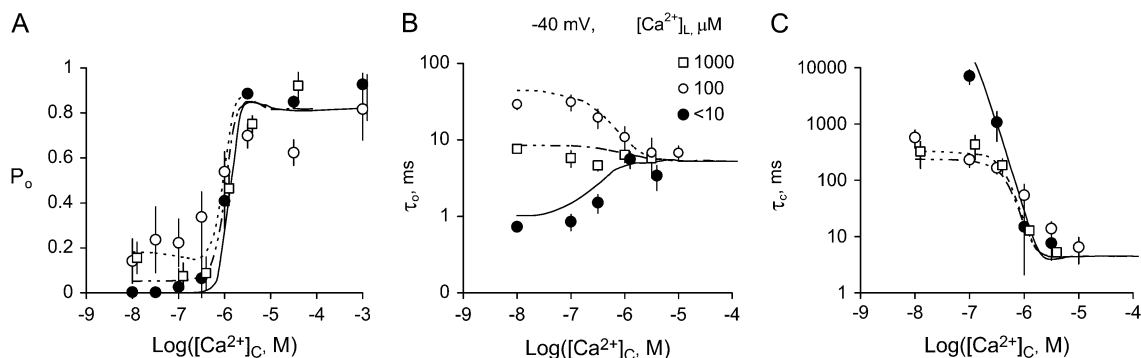


FIGURE 4 The effect of $[Ca^{2+}]_C$ on the activity of RyR₂ at -40 mV. The values P_o , τ_o , and τ_c were measured in the presence of 2 mM ATP at $[Ca^{2+}]_L < 10 \mu M$ (●), 100 μM (○), or 1000 μM (□). (A) Mean open probability P_o mean \pm SE. The numbers of experiments and the Hill parameters are listed in Table 2 (Hill fits to the data are not shown). (B, C) The mean \pm SE of three-to-eight measurements of τ_o and τ_c . The curves $[Ca^{2+}]_L < 10 \mu M$ (solid), 100 μM (short-dashes), and 1000 μM (long-dashes) show the fit to the data of the luminal-triggered Ca^{2+} feedthrough model using the parameters in Table 1.

TABLE 2 Hill parameters for cytoplasmic Ca^{2+} -activation of RyR₂ P_o

No.	Voltage mV	$[\text{Ca}^{2+}]_L$ μM	N	P_{max}	P_{min}	K_a μM	n_a
2 mM ATP							
1	-40	<10	11	0.9 ± 0.04	0.003 ± 0.04	0.9 ± 0.14	2 ± 1.3
2	-40	100	16	0.66 ± 0.18	0.20 ± 0.07	0.5 ± 0.17	2 ± 2
3	-40	1000	7	0.65 ± 0.06	0.07 ± 0.03	1.1 ± 0.16	2.4 ± 2
4	40	<10	11	0.8 ± 0.03	0.01 ± 0.04	0.7 ± 0.12	3.0 ± 2.4
5	40	100	15	0.65 ± 0.05	0.01 ± 0.05	0.6 ± 0.16	1.5 ± 1.0
6	40	1000	7	0.85 ± 0.03	0.02 ± 0.02	1.5 ± 0.25	2.2 ± 0.8
0 mM ATP							
7	-40	100	13	0.54 ± 0.13	0 ± 0.03	5.4 ± 2.0	2 ± 1.9
8	40	100	13	0.50 ± 0.06	0 ± 0.03	7.6 ± 1.7	2 ± 1.8

Examples of data are shown in Figs. 4 and 8. Parameters are described in Materials and Methods. N is the number of experiments averaged for each trace.

threefold over the experimental voltage range and this could reflect an intrinsic voltage-dependence of the RyR opening mechanism. Taken together, these results indicate that $[\text{Ca}^{2+}]_L$ -activation of opening rate is mediated by luminal facing sites of action.

The properties of the L -site are derived from the data in Fig. 6, *B* and *D*, as follows: RyR₂ opening rate associated with the L -site (α' in Scheme 1) has an asymptotic dependence on $[\text{Ca}^{2+}]_L$ (Fig. 6 *B*) that is characteristic of a two-step mechanism [$(L_C + 2\text{Ca}^{2+}) \leftrightarrow L^*_C \leftrightarrow L^*_O$] in which Ca^{2+} binding (which is relatively fast) leads to channel opening. In the absence of Ca^{2+} feedthrough, the mean duration of these openings (~ 1 ms) is determined by the closing rate, β' . The Hill coefficient for the $[\text{Ca}^{2+}]_L$ -dependence of opening rate was 1.6, suggesting a second-order dependence

of α' on $[\text{Ca}^{2+}]_L$ in Eq. 2. The voltage-dependence of V_{max} is accommodated by imposing a voltage-dependence on α' .

Characteristics of the luminal-triggered Ca^{2+} feedthrough model

The model accounts for the $[\text{Ca}^{2+}]_L$, $[\text{Ca}^{2+}]_C$, and voltage-dependencies of τ_o and τ_c over the range -60 mV to $+20$ mV (Figs. 4–6, *curves*, the model discrepancy at $+40$ mV is discussed in the section on model limitations). The model predictions of the $[\text{Ca}^{2+}]_C$ -dependencies of τ_o and τ_c , shown in Fig. 4, *B* and *C*, can be understood in terms of the various reaction steps in Scheme 4. In the absence of luminal Ca^{2+} , τ_o is primarily determined by the rates δ'_o and θ'_o of the steps $LA1_{2C} \leftarrow LA^*I_{2O} \rightarrow LA^*I^*_{2C}$. These rates have opposite $[\text{Ca}^{2+}]_C$ -dependencies

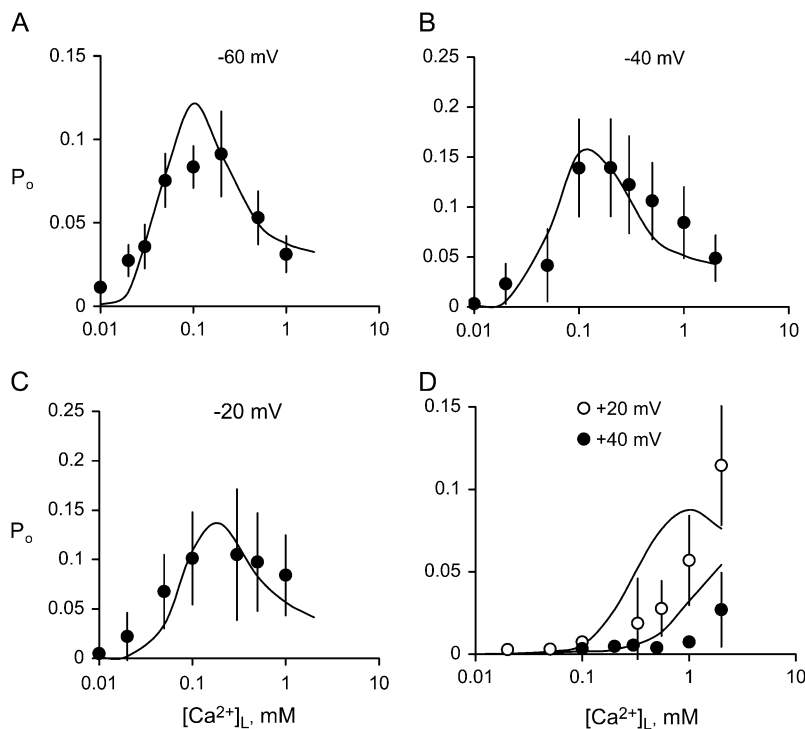


FIGURE 5 The $[\text{Ca}^{2+}]_L$ -dependence of RyR₂ P_o . (*A–D*) RyRs were activated at the voltage indicated, by 2 mM ATP and 100 nM $[\text{Ca}^{2+}]_C$. Data points show the mean \pm SE of 3–18 measurements. Solid curves show the fit to the data of the luminal-triggered Ca^{2+} feedthrough model using the parameters listed in Table 1.

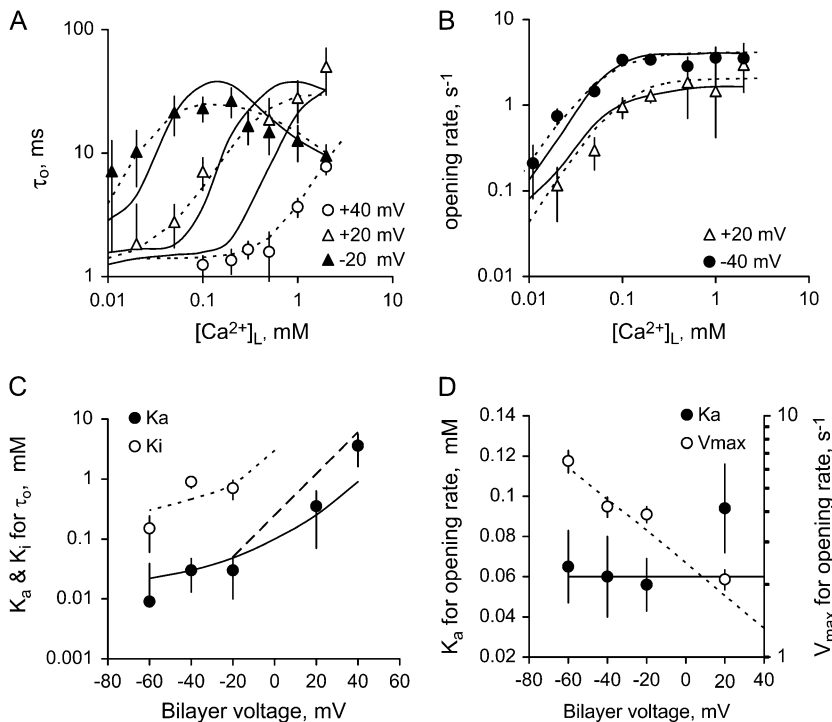


FIGURE 6 The effects of membrane potential on the $[Ca^{2+}]_L$ -dependent gating of RyR₂. (A) Mean channel open times at three membrane voltages and (B) channel opening rates at two voltages. Rates were calculated from the inverse of the mean of closed times. The data points show mean \pm SE of 3–14 measurements. In panels A and B, the dashed curves show Hill fits to the data (parameter values plotted in C and D) and the solid curves show the fits of the luminal-triggered Ca^{2+} feedthrough model using the parameters listed in Table 1. (C) Half-activating and inactivating $[Ca^{2+}]_L$, K_a (●), and K_i (○) for τ_o . (D) The K_a for RyR opening rate (●) and maximum opening rate (V_{max} , ○). The Hill coefficient for opening rate was 1.6 ± 0.3 . In panels C and D, the solid and dashed curves show the fit to the data of the luminal-triggered Ca^{2+} feedthrough model. The line (long dashes) shows the voltage-dependence in K_a expected from translocation of Ca^{2+} through the membrane voltage (i.e., where $[Ca^{2+}]_p \propto [Ca^{2+}]_L \exp(-2eV/kT)$).

and their effects on the $[Ca^{2+}]_C$ -dependence of τ_o tend to cancel, leaving a small increase in τ_o with increasing $[Ca^{2+}]_C$ (Fig. 4 B, solid curve). When $[Ca^{2+}]_L = 100 \mu M$ the L-site is mostly bound to Ca^{2+} so that τ_o is primarily determined by the inactivation transitions in $L^*AI^*_{2C} \leftarrow L^*AI_{2O} \leftrightarrow L^*A^*I_{2O} \rightarrow L^*A^*I^*_{2C}$. Under these conditions the $[Ca^{2+}]_C$ -dependent decrease in τ_o (Fig. 4 B, short dashes) reflects the Ca^{2+} -inactivation rate, θ'_o . Fig. 4 C shows the model predictions of the $[Ca^{2+}]_C$ -dependence of τ_c . At low $[Ca^{2+}]_C$ τ_c is primarily determined by α' in the reaction step $LAI_{2C} \rightarrow L^*AI_{2O}$ so that τ_c depends on $[Ca^{2+}]_L$ (compare curves at 10 μM and 100 μM $[Ca^{2+}]_L$ in Fig. 4 C). Increasing $[Ca^{2+}]_C$ decreases τ_c as γ'_c increasingly determines the channel opening rate via the reaction step $LAI_{2C} \rightarrow LA^*I_{2O}$. When $[Ca^{2+}]_C \geq 3 \mu M$, γ'_c becomes very large, then ϕ' in the reactivation step $LA^*I^*_{2C} \rightarrow LA^*I_{2O}$ determines the lower limit for τ_c at high $[Ca^{2+}]_C$. When $[Ca^{2+}]_L = 1000 \mu M$ the Ca^{2+} feedthrough is large enough to cause saturation of the I_2 -site so that $[Ca^{2+}]_C$ is unable to modulate inactivation (Fig. 4 B, long/short dashes).

The effects of $[Ca^{2+}]_L$ and voltage on τ_o and τ_c are compared with the model in Fig. 6, A and B, respectively. In the absence of Ca^{2+} feedthrough (low $[Ca^{2+}]_L$ or large positive voltage), τ_o is determined by β' in the reaction $LAI_{2C} \leftarrow L^*AI_{2O}$. The contribution of Ca^{2+} feedthrough is modeled by an extension of the former scheme: $LAI_{2C} \leftarrow L^*AI_{2O} \leftrightarrow L^*A^*I_{2O} \rightarrow L^*A^*I^*_{2C}$. Increasing Ca^{2+} feedthrough biases the state occupancies to the right so that the closing step on the left becomes less frequent. Hence, τ_o increases with $[Ca^{2+}]_L$ until the Ca^{2+} -dependent closing step on the right

becomes fast enough to decrease τ_o . According to the conductance model, the curvature in the voltage-dependencies in the log-plots in Fig. 6 C comes from saturation of I_{Ca} as the driving force on Ca^{2+} becomes large. Fig. 6 B shows the corresponding model predictions of channel opening rate at 100 nM $[Ca^{2+}]_C$. At these low $[Ca^{2+}]_C$, the channel opening rate reflects α' in the luminal activation step $LAI_{2C} \rightarrow L^*AI_{2O}$. The luminal site affinity (K_L) determines the $[Ca^{2+}]_L$ range for the rising phase in the opening rate.

In addition to τ_o and τ_c , it was found that the model could also account for the effect of $[Ca^{2+}]_L$ on the shape of the dwell-time distributions in the presence of low $[Ca^{2+}]_C$. Fig. 7 shows the distribution of channel open and closed times at three $[Ca^{2+}]_L$ representing the subactivating (10 μM), maximal-activating (100 μM), and inactivating regions (1 mM) of the bell-shaped dependence of RyR₂ activity on $[Ca^{2+}]_L$ (−40 mV, $[Ca^{2+}]_C = 100$ nM). The shape of the closed time distributions varied considerably with $[Ca^{2+}]_L$ (Fig. 7, A, C, and E). As $[Ca^{2+}]_L$ increased, the time-constant of the main exponential component decreased from 10 s to 200 ms and the distribution changed from unimodal to bimodal with the appearance of another time constant of ~ 1 ms. Open time distributions (Fig. 7 B, D, and F) were double exponentials as described in Fig. 3. Although the peak of the log-binned open distributions depended on $[Ca^{2+}]_L$, the shape of the distributions was similar over the experimental range. The model faithfully reproduced the effect of $[Ca^{2+}]_L$ on these dwell time distributions (Fig. 7, curves). According to the model, closure of the channel causes termination of Ca^{2+} feedthrough which, at low $[Ca^{2+}]_C$, leads to deactivation of

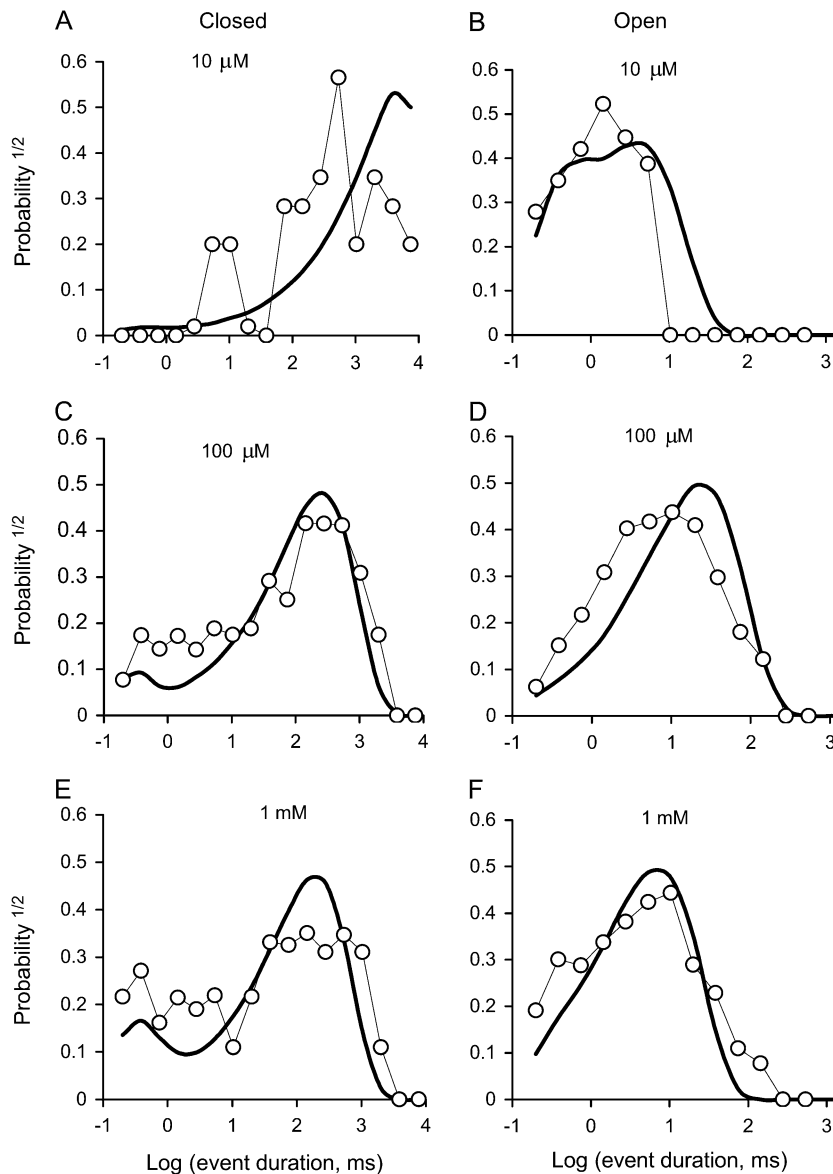


FIGURE 7 The effect of $[Ca^{2+}]_L$ on closed (A, C, and E) and open (B, D, and F) dwell-time distributions. The data are plotted using the log-bin method of Sigworth and Sine (22). Event duration distributions were compiled from a single RyR, which was activated by cytoplasmic 2 mM ATP (100 nM $[Ca^{2+}]_C$ and voltage = -40 mV) and the indicated $[Ca^{2+}]_L$. The data are plotted using log-bins with 3.5 per decade. Solid curves show simulated distributions generated from the luminal-triggered Ca^{2+} feedthrough model using the parameters listed in Table 1.

the RyR via Ca^{2+} dissociation from the A-site, underlying the long closed events. By the same process, channel closures allow Ca^{2+} dissociation from the I_2 -site, which permits reopening of the channel. The 1-ms time constant in the closed dwell-time distributions is associated with instances of recovery from I_2 -site inactivation that occurred before the channel had time to deactivate.

The effect of ATP on activation by $[Ca^{2+}]_C$ and $[Ca^{2+}]_L$

The effects of ATP are reexamined here in the light of the new Ca^{2+} regulation model. Fig. 8 compares the $[Ca^{2+}]_C$ -dependent properties of RyR₂ in the presence and absence of ATP. ATP increased P_o over the entire experimental range of $[Ca^{2+}]_C$ (Fig. 8 A). It increased the maximal activation at

high $[Ca^{2+}]_C$ (P_{max}), decreased the $[Ca^{2+}]_C$ for half-activation (K_a), and altered P_o at subactivating $[Ca^{2+}]_C$ (P_{min}) depending on $[Ca^{2+}]_L$ and voltage (Table 2). In accord with previous findings (30), ATP activated RyRs through an increase in τ_o and a decrease in τ_c (Fig. 8, B and C). In the virtual absence of Ca^{2+} feedthrough ($+40$ mV), $[Ca^{2+}]_C$ caused a much bigger increase in τ_o and P_o in the presence of ATP than in its absence.

Fig. 9 compares the $[Ca^{2+}]_L$ -dependent properties of RyR₂ in the presence and absence of ATP. Also, as previously reported, ATP markedly amplified the effects of $[Ca^{2+}]_L$ on P_o (at low $[Ca^{2+}]_C$, Fig. 9 A). In the presence of ATP (-40 mV), τ_o showed a bell-shaped dependence on $[Ca^{2+}]_L$ whereas in the absence of ATP, τ_o remained relatively constant (Fig. 9 B). It is interesting to note that ATP had similar effects on the $[Ca^{2+}]_L$ - and $[Ca^{2+}]_C$ -dependencies

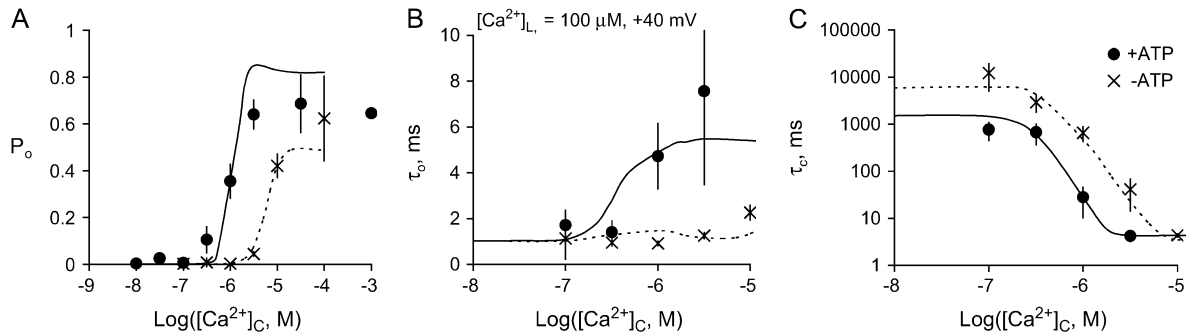


FIGURE 8 The effect of ATP and $[Ca^{2+}]_C$ on the activity of RyR₂ at +40 mV. The values P_o , τ_o , and τ_c were measured in the presence of 2 mM ATP (●) and in its absence (×). (A) Mean open probability P_o mean \pm SE. The numbers of experiments and the Hill parameters are listed in Table 2 (Hill fits to the data are not shown). (B, C) The mean \pm SE of 3–9 measurements of τ_o and τ_c . The curves (2 mM ATP, *solid*; and absence of ATP, *dashed*) show the fits of the luminal-triggered Ca^{2+} feedthrough model using the parameters in Table 1.

of τ_o in that, in both cases, an increase in Ca^{2+} could only increase τ_o when ATP was present. This is consistent with common sites of action for cytoplasmic and luminal Ca^{2+} . K_a for opening rate was not significantly affected by ATP (Fig. 9 B), indicating that ATP did not modify the affinity of the L-site. Rather, ATP appeared to stabilize the open state of the channel and destabilize the closed state.

In the model, the ability of ATP to increase τ_o in response to Ca^{2+} binding at the A-site is encapsulated in the parameter n in Eqs. 5 and 7a. In the presence of ATP, $\tau_o \propto [Ca^{2+}]_C$ (Fig. 8 B, *solid circle*), which is indicative of the channel closing rate, $\delta \propto [Ca^{2+}]_C^{-1}$ (i.e., $n = 1$). In the absence of ATP, τ_o is nearly independent of $[Ca^{2+}]_C$ (Fig. 8 B, ×) so that $n = 0$. The larger τ_c in the absence of ATP (Fig. 8 C, ×) is accommodated in the model by a 13-fold decrease in the opening rate constant associated with the A-site, γ (see Table 1).

The model predictions for the $[Ca^{2+}]_L$ -dependencies of τ_o and τ_c in the absence of ATP can be explained along similar lines to those presented above for ATP-activated RyRs. The contribution of Ca^{2+} feedthrough to τ_o depends on the steps $LAI_{2C} \leftarrow L^*AI_{2O} \leftrightarrow L^*A^*I_{2O} \rightarrow L^*A^*I_{2C}$. However, in the absence of ATP the states $L^*A^*I_{2O}$ and L^*AI_{2O} have

approximately the same average duration. Therefore, although Ca^{2+} feedthrough biases the state occupancies to the right, in the absence of ATP this causes no significant increase in τ_o . Fig. 9 B shows the corresponding model predictions of channel opening rate. The decreased $[Ca^{2+}]_L$ -dependent opening rate in the absence of ATP was accommodated by a decrease in α' in the luminal activation step $LAI_{2C} \rightarrow L^*AI_{2O}$.

Ca^{2+} feedthrough couples RyR₂ in lipid bilayers

In six instances, vesicle fusion events incorporated clusters of 3–6 RyR₂ into the bilayer. At subactivating $[Ca^{2+}]_C$ (100 nM Ca^{2+} and 2 mM ATP) and when conditions favored Ca^{2+} feedthrough, the opening of one RyR tended to promote the opening of other RyRs (i.e., channels displayed coupled gating). Fig. 10 shows a recording of six RyRs at positive and negative bilayer potentials. The current trace shows transitions between the current baseline (labeled C for closed) and equally spaced levels corresponding to 1–6 open channels. At –40 mV, channel openings were clearly grouped into bursts and the weighting of current levels in these records markedly deviated from a binomial distribution

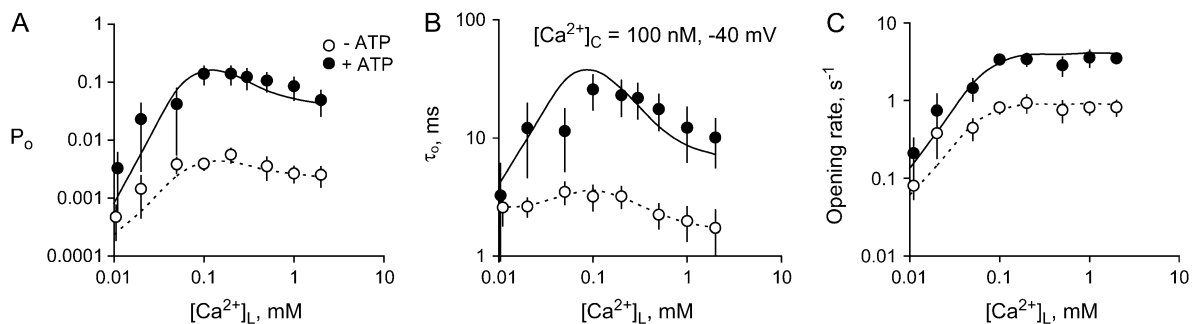


FIGURE 9 The effects of ATP on the $[Ca^{2+}]_L$ -dependent gating of RyR₂. (A) The open probability of RyRs (100 nM $[Ca^{2+}]_C$ and voltage = –40 mV) in the presence of 2 mM ATP (●) and in its absence (○). Also shown are the corresponding τ_o (B) and opening rates (C). Solid and dashed curves show the fit to the data of the luminal-triggered Ca^{2+} feedthrough model using the parameters listed in Table 1. The data points show mean \pm SE of 3–18 measurements. Hill fits (not shown) to the opening rate reveal that 2 mM ATP increases V_{max} from 0.8 ± 0.1 to 4.0 ± 0.4 without significantly changing K_a ($K_a = 45 \pm 8 \mu M$ and $60 \pm 20 \mu M$ in the absence and presence of ATP, respectively).

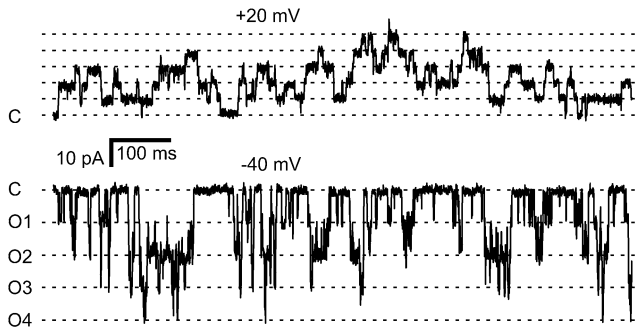


FIGURE 10 Recordings from an experiment with six RyRs in the bilayer showing coupled gating. At +20 mV (*top trace*), the channels appeared to gate independently. The dashed lines indicated the current levels associated with various numbers of open channels. The closed current level is labeled C. At -40 mV (*bottom trace*), the opening of a single channel (transitions from C to O1) was followed closely by openings to higher levels. Only four levels are apparent in this section (labeled O1–O4). The baths contained symmetric 250 mM Cs⁺ solutions with 2 mM ATP, [Ca²⁺]_C = 100 nM, and [Ca²⁺]_L = 1 mM.

(not shown). Hidden Markov Model analysis of these records (see Materials and Methods) showed that the mean RyR opening rate associated with transitions between the current baseline and level O1 was $\sim 10\times$ slower than opening rates associated with transitions between higher levels (Fig. 11 A, *solid circle*). Channel closing rates did not depend on the number of open RyRs (Fig. 11 B). Thus, RyR coupling appeared to be mediated by the opening rates. The degree of channel coupling was substantially reduced by decreasing [Ca²⁺]_L from 1 mM to 0.1 mM or by application of positive bilayer potentials (Fig. 11 A), conditions that oppose Ca²⁺ feedthrough. These results are consistent with the notion that the opening of one channel in the bilayer permits Ca²⁺ feedthrough that can trigger the opening of neighboring RyRs via their A-sites. The luminal-triggered Ca²⁺ feedthrough model was extended to include this possibility by introducing another parameter, Z, which describes the proportionality between I_{Ca} and its effect on [Ca²⁺]_P at a neighboring channel. The predicted opening and closing rates for the first opening in a cluster were calculated the same way as for single RyRs. The rates associated with the n^{th} channel opening were calculated using a value for

[Ca²⁺]_P in Eqs. 7b and 10b that incorporated the additional term, $(n - 1)ZI_{Ca}$.

The model predictions are compared with the data using a Z value of 0.3. Given the experimental buffering conditions, this corresponds to an interpore separation of ~ 3 nm, which corresponds to the separation of neighboring RyR pores in the triad junction (31). Although the model tends to underestimate the gating rates, it does give a qualitative account of voltage- and [Ca²⁺]_L-dependent coupling via channel opening rates. In the model, the first channel opening in the cluster is controlled as described for single RyRs (see above). Thus, at 100 nM [Ca²⁺]_C, 1 mM [Ca²⁺]_L, and -40 mV, luminal Ca²⁺ binding to the L-site is the primary trigger for channel opening whereas Ca²⁺ feedthrough serves to reinforce the stability of channel opening. However, the primary trigger for subsequent channel openings is the A-site because feedthrough from the first open channel elevates [Ca²⁺]_P to 1–3 μ M. At these [Ca²⁺]_C, channel opening rates via the A-site are more than 10-fold higher than those attainable via the luminal L-site. In the model, the channel closing rates are slightly increased by the opening of neighboring channels because Ca²⁺ feedthrough also contributes to inactivation of neighboring RyRs via I₂-sites.

Model limitations

The luminal-triggered Ca²⁺ feedthrough model accounts for the Ca²⁺ regulation of RyR₂ by the actions of three Ca²⁺ binding sites that are linked by Ca²⁺ flowing through the pore. However, other Ca²⁺ regulation mechanisms could also play a role in controlling Ca²⁺ release from the SR. For example, the model does not include the low affinity Ca²⁺/Mg²⁺ inhibition mechanism (18). In addition, the [Ca²⁺]_C-activation mechanism is known to be complex and involves several Ca²⁺-dependent steps (24,25). Simplification of this into A- and I₂-site gating mechanisms should make the model unsuitable for predicting the complex shape of the dwell-time distributions. With this in mind, it is surprising that the model accounts so well for the [Ca²⁺]_L-dependent dwell-time distributions at subactivating [Ca²⁺]_C (Fig. 7). There is also the possibility that the L-site modulates the RyR in other

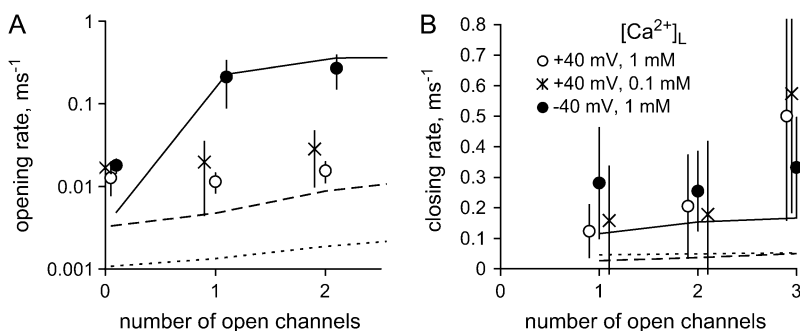


FIGURE 11 The dependence of mean channel opening rate (A) and closing rate (B) on the number of open channels. Rates were measured in the presence of 2 mM ATP and 100 nM [Ca²⁺]_C. Opening rates were significantly increased ($P < 0.05$, *t*-test) by the presence of other open channels under conditions that favored Ca²⁺ feedthrough (●, -40 mV [Ca²⁺]_L = 1 mM, six measurements). When Ca²⁺ feedthrough was relatively low, this did not occur (○, +40 mV [Ca²⁺]_L = 1 mM; ×, -40 mV [Ca²⁺]_L = 0.1 mM, three measurements each). Closing rates did not significantly depend on the presence of other open channels in the bilayer. The data are compared with predictions of the luminal-triggered Ca²⁺ feedthrough model: ●, solid line; ×, long dashes; ○, dashed line.

ways than merely causing channel opening. An example of this has recently been reported in RyR₁ (14) where a luminal Ca²⁺ binding site was shown to modulate the A-site affinity for Mg²⁺ (preliminary data indicates that this phenomenon does not occur in RyR₂).

As yet, there has been no direct measure of the Ca²⁺ current under experimental conditions. Therefore, I_{Ca} is estimated from rate theory calculations based on an energy barrier model of the RyR pore (27). A possible failure of the energy barrier model to accurately predict I_{Ca} under some conditions could underlie the deviation of the model from the data (see the voltage-dependence in τ_o that occurred between +20 mV and +40 mV in Fig. 6, A and C). The rate theory model provided a good prediction of the total current in the channel (Cs⁺ plus Ca²⁺ in this instance, not shown). However, at +40 mV, I_{Ca} is relatively small and only represents ~1% of the total current. Therefore, it is possible for the model to accurately predict the total current and yet be an order-of-magnitude out in estimating I_{Ca} . Just a twofold error in I_{Ca} would account for the deviations between the model and the data at +40 mV. Interestingly, τ_o at positive voltages could be better explained by a voltage-dependent equilibrium between Ca²⁺ on either end of the pore in which $[Ca^{2+}]_p \propto [Ca^{2+}]_L \exp(-2eV/kT)$ (Fig. 6 C, long dashes). In any case, the luminal-triggered Ca²⁺ feedthrough model provides a good fit to the data between -60 mV and +20 mV, which encompasses the membrane potential of the SR (0 mV, (32)).

The extension of the luminal-triggered Ca²⁺ feedthrough model to coupled RyR clusters involved a number of assumptions that are yet to be validated. In the model, coupling occurs between nearest neighbors, although it could also occur between more remote pores. It is not clear that, in the bilayer, RyRs do form the same arrays as they do in muscle. The model assumes that the action of Ca²⁺ feedthrough on neighboring channels can be predicted by the steady-state action of raised $[Ca^{2+}]_C$. However, neighboring RyRs would be stimulated by a rapid stepwise increase in $[Ca^{2+}]_C$ and it is known that RyRs can exhibit gating properties that are peculiar to non-steady-state situations (33,34).

DISCUSSION

The results obtained here support the proposition that RyR activation by Ca²⁺ stores is due to Ca²⁺ binding sites on both the luminal and cytoplasmic sides of the channel. This study shows that store regulation of RyRs and ER/SR excitability involves three modes of action associated with different parts of the RyR molecule; the L-site, A-site, and I₂-site (Fig. 1). The L- and I₂-sites have not been previously identified and this study makes the first measurement of their properties. The effects of $[Ca^{2+}]_L$ on opening rate in Fig. 6, B and C, highlight the existence of a luminal-facing Ca²⁺ activation site (L-site) with an affinity of 60 μ M. The binding of Ca²⁺ to the L-site on its own can activate channel open-

ings of ~1 ms duration at rates of ~1–10 s⁻¹. Once the channel is open, the flux of Ca²⁺ from the luminal to cytoplasmic sides of the channel increases the cytoplasmic $[Ca^{2+}]$ near the A-site and produces up to 30-fold prolongation of channel openings. Thus, a large component of the RyR activation by luminal Ca²⁺ (up to 97%) is due to the effects of Ca²⁺ feedthrough. However, without the luminal site to trigger the initial channel openings, activation by $[Ca^{2+}]_L$ would not occur. Therefore, the proposed mechanism for store activation of RyRs is luminal-triggered Ca²⁺ feedthrough, incorporating both the true luminal and feedthrough hypothesis. This hybrid mechanism would explain the apparently contradictory findings whereby enzyme digestion of luminal RyR domains abolishes luminal Ca²⁺ activation (13), but there is a close correlation between RyR activity and Ca²⁺ flux through the pore (10).

Ca²⁺-inactivation

This study makes the first demonstration in single channel recording of a high affinity, $[Ca^{2+}]_C$ -dependent inactivation in RyRs. It is manifest as a Ca²⁺-dependent reduction in channel τ_o (Figs. 2 A and 4 B). The affinity of the I₂-site is ~1.2 μ M, which is similar to that of the A-site (0.9 μ M) so that both activation and inactivation occur over the same range of $[Ca^{2+}]_C$. $[Ca^{2+}]_C$ -activation overrides the effects of the I₂-site, which causes $\leq 20\%$ reduction in P_o in response to cytoplasmic Ca²⁺. However, the I₂-site causes up to 98% reduction in P_o in response to feedthrough of luminal Ca²⁺ in the presence of physiological (100 nM) $[Ca^{2+}]_C$. This is because channel closures block Ca²⁺ feedthrough, leading to deactivation via the A-site and substantial lengthening of closed events.

It is well known that cytoplasmic Ca²⁺ and Mg²⁺ cause identical inhibition of RyRs at high concentrations (~1 mM for RyR₁ and ~10 mM for RyR₂ (35)). This inhibitory action is mediated by a low affinity nonspecific cation site (I₁-site, previously named the I-site). It was thought that inactivation by high $[Ca^{2+}]_L$ was mediated by Ca²⁺ feedthrough to the I₁-site (11) because until now, the I₁-site was the only Ca²⁺-dependent inhibition mechanism that had been clearly identified in RyRs. It is unlikely that the I₁-site causes inactivation by high $[Ca^{2+}]_L$ because inactivation has a similar $[Ca^{2+}]_L$ sensitivity in RyR₁ and RyR₂ (see (11) and (10)) whereas the Ca²⁺ sensitivity of the I₁-site differs 10-fold between the two isoforms. Moreover, the I₁-site shows no specificity between Ca²⁺ and Mg²⁺, whereas the luminal inhibition via the I₂-site is ~100-fold less sensitive to Mg²⁺ than to Ca²⁺ (unpublished data).

Accessibility of A- and I₂-sites to luminal Ca²⁺

It is noteworthy that even though the A- and I₂-sites have similar affinity for cytoplasmic Ca²⁺, the effects of luminal

Ca^{2+} on these sites occur over quite different ranges of $[\text{Ca}^{2+}]_{\text{L}}$. The model indicates that the feedthrough effects of Ca^{2+} are ~ 40 -fold larger for the *A*-site than for the *I*₂-site (see *X* and *Y* in Table 1), which suggests a marked difference in the accessibility of these sites to luminal Ca^{2+} . This difference is readily explained by the relative proximity of these sites to the Ca^{2+} pore (10). Ca^{2+} emanating from the pore will diffuse into the cytoplasm and be sequestered by buffering molecules (4.5 mM BAPTA). This leads to a decline in $[\text{Ca}^{2+}]$ with distance from the pore (see Eq. 1). The luminal-triggered Ca^{2+} feedthrough model predicts that each pA of Ca^{2+} current through the channel causes a 15 μM increase in $[\text{Ca}^{2+}]$ at the *A*-site and a 0.35 μM increase at the *I*₂-site (e.g., $I_{\text{Ca}} = 4.9$ pA at -40 mV when $[\text{Ca}^{2+}]_{\text{L}} = 1$ mM hence $[\text{Ca}^{2+}]_{\text{p}} = 73$ μM at the *A*-site and 1.7 μM at the *I*₂-site). This places the *A*- and *I*₂-sites at 11 nm and 26 nm from the pore, respectively. Given that the furthest point on the RyR from the pore is ~ 20 nm (36), it would seem that the *I*₂-sites are located at the periphery of the protein or perhaps on an adjacent inhibitory protein. The relative proximity of the *A*- and *I*₂-sites to the pore is in accord with the observation that Ca^{2+} buffering of the cytoplasmic bath affects inactivation much more strongly than activation (10).

Cytoplasmic agonists and luminal Ca^{2+} activation

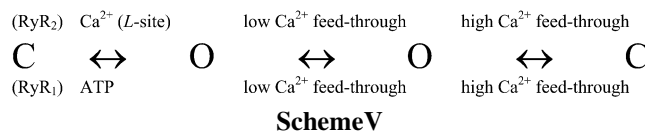
Several studies have shown that $[\text{Ca}^{2+}]_{\text{L}}$ -dependent activation of RyRs is mainly seen in the presence of agonists such as ATP, caffeine, or sulmazole (8,28,29). Previously it was proposed that these agonists unmask a luminal Ca^{2+} sensing site (6). The luminal-triggered Ca^{2+} feedthrough model points to a different mechanism in which the *L*-site affinity is not altered by agonists. Rather, they stabilize the channel open conformation, destabilize the closed conformation, and, in conjunction with Ca^{2+} feedthrough, markedly increase channel activation in response to $[\text{Ca}^{2+}]_{\text{L}}$.

One of these agonists, ATP, is shown here to enhance $[\text{Ca}^{2+}]_{\text{L}}$ -activation of RyR₂ by three modes of action. Firstly, ATP increases the rate of opening of RyRs that occurs in response to Ca^{2+} binding at the *L*-site (Fig. 9 C). Secondly, in accord with previous findings (37), ATP is a cofactor that causes τ_o to increase in response to Ca^{2+} binding at the *A*-site. Therefore, Ca^{2+} feedthrough should increase τ_o in the presence of ATP, whereas in the absence of ATP, τ_o should not be altered. The results show this to be the case (Fig. 9 B). Thirdly, ATP decreases the rate of inactivation via the *I*₂-site. In regard to the last two actions, the effects of ATP on the $[\text{Ca}^{2+}]_{\text{L}}$ -dependence of τ_o were entirely consistent with Ca^{2+} feedthrough and the observed effects of ATP on the $[\text{Ca}^{2+}]_{\text{C}}$ -dependence of τ_o (Fig. 9, *dashed* and *solid* curves).

Previous studies (30,38–40) have shown that cytoplasmic agonists such as caffeine and ATP have quite different effects on RyR gating than Ca^{2+} . Caffeine and ATP produce a much lower P_o and they generate much longer channel openings and closures than Ca^{2+} (Fig. 2 A, see *top trace* showing an RyR

activated by ATP with *bottom trace* of an RyR activated by Ca^{2+} and ATP). The different forms of activation by Ca^{2+} and ATP can be understood in terms of the luminal-triggered Ca^{2+} feedthrough model. Firstly, cytoplasmic Ca^{2+} activation via the *A*-site can cause much faster activation rates than ATP, which is limited by the triggering of openings by the *L*-site (hence the longer τ_c and the lower P_{max} with ATP relative to Ca^{2+}). Secondly, channels activated by cytoplasmic Ca^{2+} are more affected by *I*₂-site mediated inactivation than ATP-activated RyRs (hence τ_o is longer ATP than with Ca^{2+}).

Another prediction of the model is that cardiac and skeletal RyR isoforms are differently regulated by luminal Ca^{2+} . It is known that there are marked differences in the ways that RyR₁ and RyR₂ are regulated by the cytoplasmic milieu (41). Of particular relevance is that RyR₁ and RyR₂ are differently regulated by cytoplasmic ATP. RyR₁ can be activated by ATP in the absence of cytoplasmic and luminal Ca^{2+} (10,14). However, as shown here and elsewhere (28, 42), ATP acts as a cofactor on RyR₂, which increases its activation in response to Ca^{2+} but does not in itself trigger channel openings. This difference in ATP regulation underlies important differences in the way that RyR₁ and RyR₂ respond to luminal Ca^{2+} (see Scheme V). It is proposed here that opening of RyR₂ at 100 nM $[\text{Ca}^{2+}]_{\text{C}}$ is primarily triggered by Ca^{2+} binding to the *L*-site whereas Ca^{2+} feedthrough serves to reinforce stability of channel opening. However, in RyR₁, cytoplasmic ATP will trigger channel openings so that the *L*-site is bypassed, resulting in a mechanism that is identical to that previously proposed for RyR₁ (10). It is possible that in the absence of ATP, RyR₁ would default to the RyR₂ mechanism for luminal Ca^{2+} regulation provided that RyR₁ also has an *L*-site.



More generally, this model predicts that any cofactor that prolongs channel openings triggered by cytoplasmic Ca^{2+} will promote RyR activation by luminal Ca^{2+} (the converse will be true for cytoplasmic antagonists). This might be highly relevant to the effects of RyR₂ mutations associated with Sudden Cardiac Death, which are known to enhance activation by luminal Ca^{2+} (43) and the ability of polyunsaturated fatty acids, which are RyR antagonists, to protect myocardium against store-overload-induced arrhythmias (44,45). A number of RyR₂ co-proteins have been found to modify $[\text{Ca}^{2+}]_{\text{L}}$ -regulation of RyRs. The luminal Ca^{2+} buffering protein, calsequestrin (CSQ), along with triadin and junctin, are known to bind to RyR₂ and confer luminal Ca^{2+} activation, thus being considered as the luminal Ca^{2+} sensor (46). However, it is not yet clear if these proteins constitute the *L*-site itself or whether they merely act as a

cofactor that prolongs the channel openings triggered by $[Ca^{2+}]_C$. In addition, CSQ dissociation from RyR₂ could be a sensor for Ca^{2+} overload of the SR. Exposure of RyR₂ in bilayers to 5 mM $[Ca^{2+}]_L$ caused a substantial increase in their activity via CSQ dissociation (46). Earlier studies by the same authors found the same treatment caused an increase in the Ca^{2+} affinity of the *A*-site (29). In this study $[Ca^{2+}]_L$ was kept below 2 mM to minimize the possibility of CSQ dissociation from the RyR. Another cytoplasmic protein, calmodulin (CAM), decreases RyR₂ sensitivity to $[Ca^{2+}]_C$ via the *A*-site and appears to modify the action of Ca^{2+} feedthrough on RyR₂ activity (47). It is unlikely that CAM contains the *A*- or *I*₂-sites since CAM was not present in this study. CAM is rapidly dissociated from RyRs by the mM $[Ca^{2+}]$ used to promote SR vesicle fusion with the bilayer.

Coupled gating of RyR₂ in muscle

The coupled opening of RyRs observed here is very similar to the phenomenon reported previously in RyR₁ and RyR₂ (14,16,17), where it was proposed that coupling occurred when Ca^{2+} flow through one channel raised the local $[Ca^{2+}]_C$ sufficiently to activate neighboring RyRs. This was based on the findings that 1), the coupling only occurred under conditions favoring Ca^{2+} feedthrough; 2), coupling did not occur in the presence of a strong cytoplasmic triggering stimulus ($[Ca^{2+}]_C = 100 \mu M$); and 3) the opening of one channel caused an approximately fivefold reduction in Mg^{2+} -inhibition of the other RyRs, suggesting that local $[Ca^{2+}]_C$ is indeed increased and is competing with Mg^{2+} for the *A*-sites. In this study, RyR₂ coupling was also promoted under conditions favorable to Ca^{2+} feedthrough. The coupling of RyR₂ seen here differed slightly from those reported in RyR₁. There was a much larger relative difference between the first and second opening rates in RyR₂ than RyR₁ (compare 10× for RyR₂ versus 2× for RyR₁). This probably reflects the different ligand sensitivities of the two isoforms. RyR₁ is more strongly stimulated by ATP than RyR₂ so that the initial opening rate for RyR₁ in a cluster is much higher. However, the rate of subsequent channel openings for RyR₁ and RyR₂ are similar because both isoforms have similar sensitivity to cytoplasmic Ca^{2+} .

Ca^{2+} sparks are believed to arise from the coupled activation of up to 10 RyRs in the triad junction (15). Freeze fracture electron micrographs show that RyRs within the triad junction are organized into square, two-dimensional arrays (31). The coupling between RyR openings in lipid bilayer experiments suggests that during SR vesicle isolation and reconstitution, fragments of these RyR arrays are retained. The model for luminal-triggered Ca^{2+} feedthrough highlights the different mechanisms that might underlie the frequency and morphology of Ca^{2+} sparks. Spark frequency is likely to be governed by the opening rate of RyRs in the absence of any open channels, whereas spark morphology would depend on coupling between RyRs. The precise role

of the *L*-, *A*-, and *I*₂-sites in regulating RyR₂ in the cell is likely to depend on how intracellular Mg^{2+} interacts with these sites. The free $[Mg^{2+}]$ in the cytoplasm and lumen is ~ 1 mM and this level of Mg^{2+} has been shown to lower the apparent Ca^{2+} affinity of the *A*-site to $\sim 10 \mu M$ (11) and the *L*-site to 500 μM (unpublished observations). In the case of the *L*-site, this places the affinity right in the middle of the physiological range of luminal Ca^{2+} .

In vivo, a Ca^{2+} spark can occur spontaneously or be initiated by the opening of a single *L*-type Ca^{2+} channel in the sarcolemma (induced sparks) (1). The results here suggest that sparks can be triggered by either binding of luminal Ca^{2+} to the *L*-site (spontaneous sparks) or binding of cytoplasmic Ca^{2+} to the *A*-site (induced and spontaneous sparks). According to the model, spark frequency is governed by the sum of the opening rates associated with *L*-site and *A*-sites. Hence spark frequency should increase with SR Ca^{2+} load or with increased cytoplasmic Ca^{2+} activation. This is consistent with the finding that spark frequency increases with increasing luminal and cytoplasmic stimuli (48,49). In permeabilized cardiac cells, ATP depletion in the presence of 200 nM $[Ca^{2+}]_C$ was shown to decrease the frequency of spontaneous sparks by >90% even though the Ca^{2+} load of the SR was increased (49). This is consistent with bilayer experiments showing that removal of ATP results in a fivefold decrease in RyR opening rate via the *L*-site (compare $\alpha \pm$ ATP in Table 1; at 200 nM $[Ca^{2+}]_C$ the *L*-site is the main trigger for RyR openings). Interestingly, some RyR activators and inhibitors have only transient effects on spark frequency because any initial change in RyR₂ activity results in an opposing change in SR Ca^{2+} load, a process dubbed autoregulation. Why this happens for caffeine and tetracaine (48) and not for ATP (49) is still a mystery. The answer might be found in knowledge of the relative effects of these substances on the *L*- and *A*-sites.

According to the model, sparks triggered by either the *L*-site or *A*-site should have the same morphology because in either case the subsequent activity of RyRs is governed by the binding of feedthrough Ca^{2+} to the *A*-site and *I*₂-sites. The *A*-sites mediate the coordinated opening of RyRs in a spark and the *I*₂-sites govern their termination. Model calculations (not shown) indicate that an *I*₂-site inactivation rate of 1000 s⁻¹ (fourfold higher than measured here) would explain the amplitude distribution and duration of sparks reported by Wang et al. (15). Whether these mechanisms indeed control spark morphology is yet to be determined.

In conclusion, RyRs possess a luminal site for Ca^{2+} -activation with an affinity of 60 μM (*L*-site) and cytoplasmic sites for Ca^{2+} -activation and Ca^{2+} -inactivation that have $\sim 1 \mu M$ affinity (*A*- and *I*₂-sites). Store Ca^{2+} regulates RyR activity by binding to the *A*-, *L*-, and *I*₂-sites and substances that alter channel gating associated with any of these sites will alter the regulation of RyRs by luminal Ca^{2+} . A unifying kinetic model is developed that makes the first quantitative predictions of Ca^{2+} permeability of the ER/SR. This model provides a framework for understanding the

mode of action of pharmacological agents (e.g., ATP and caffeine), RyR-associated proteins (e.g., calsequestrin), and RyR₂ mutations (e.g., those associated with sudden cardiac death) on a whole range of Ca²⁺ mediated physiological and pathological processes.

Sheep hearts were provided by Dr. Tony Quail. Thanks to Drs. Graham Lamb, Dirk vanHelden, and Liz Milward for critically reading the article and to Paul Johnson, Melissa Dafo, Bronwyn Hiles, and Katherine Bradley for assisting with the experiments.

D.R.L. was supported by a Senior Brawn Fellowship from the University of Newcastle. This work was supported by the Australian Research Council (grant No. DP0557780) and by an infrastructure grant from NSW Health through Hunter Medical Research Institute.

REFERENCES

- Stern, M. D., and H. Cheng. 2004. Putting out the fire: what terminates calcium-induced calcium release in cardiac muscle? *Cell Calcium*. 35:591–601.
- Coombes, S., R. Hinch, and Y. Timofeeva. 2004. Receptors, sparks and waves in a fire-diffuse-fire framework for calcium release. *Prog. Biophys. Mol. Biol.* 85:197–216.
- Fabiato, A., and F. Fabiato. 1977. Calcium release from the sarcoplasmic reticulum. *Circ. Res.* 40:119–129.
- Ford, L. E., and R. J. Podolsky. 1972. Calcium uptake and force development by skinned muscle fibers in EGTA buffered solutions. *J. Physiol. (Lond.)*. 223:1–19.
- Verkhatsky, A. 2005. Physiology and pathophysiology of the calcium store in the endoplasmic reticulum of neurons. *Physiol. Rev.* 85: 201–279.
- Sitsapesan, R., and A. J. Williams. 1997. Regulation of current flow through ryanodine receptors by luminal Ca²⁺. *J. Membr. Biol.* 159: 179–185.
- Györke, S., I. Györke, V. Lukyanenko, D. Terentyev, S. Viatchenko-Karpinski, and T. F. Wiesner. 2002. Regulation of sarcoplasmic reticulum calcium release by luminal calcium in cardiac muscle. *Front. Biosci.* 7:d1454–d1463.
- Sitsapesan, R., and A. J. Williams. 1994. Regulation of the gating of the sheep cardiac sarcoplasmic reticulum Ca²⁺-release channel by luminal Ca²⁺. *J. Membr. Biol.* 137:215–226.
- Sitsapesan, R., and A. J. Williams. 1995. The gating of the sheep skeletal sarcoplasmic reticulum Ca²⁺-release channel is regulated by luminal Ca²⁺. *J. Membr. Biol.* 146:133–144.
- Tripathy, A., and G. Meissner. 1996. Sarcoplasmic reticulum luminal Ca³⁺ has access to cytosolic activation and inactivation sites of skeletal muscle Ca²⁺ release channel. *Biophys. J.* 70:2600–2615.
- Xu, L., and G. Meissner. 1998. Regulation of cardiac muscle Ca²⁺ release channel by sarcoplasmic reticulum luminal Ca²⁺. *Biophys. J.* 75:2302–2312.
- Herrmann-Frank, A., and F. Lehmann-Horn. 1996. Regulation of the purified Ca²⁺-release channel/ryanodine receptor complex of skeletal muscle sarcoplasmic reticulum by luminal calcium. *Pflugers Arch.* 432: 155–157.
- Ching, L. L., A. J. Williams, and R. Sitsapesan. 2000. Evidence for Ca²⁺ activation and inactivation sites on the luminal side of the cardiac ryanodine receptor complex. *Circ. Res.* 87:201–206.
- Laver, D. R., E. R. O'Neill, and G. D. Lamb. 2004. Luminal Ca²⁺-regulated Mg²⁺ inhibition of skeletal RyRs reconstituted as isolated channels or coupled clusters. *J. Gen. Physiol.* 124:741–758.
- Wang, S. Q., M. D. Stern, E. Rios, and H. Cheng. 2004. The quantal nature of Ca²⁺ sparks and in situ operation of the ryanodine receptor array in cardiac cells. *Proc. Natl. Acad. Sci. USA.* 101:3979–3984.
- Laver, D. R. 2006. Regulation of ryanodine receptors from skeletal and cardiac muscle during rest and excitation. *Clin. Exp. Pharmacol. Physiol.* 33:1107–1113.
- Laver, D. R. 2005. Coupled calcium release channels and their regulation by luminal and cytosolic ions. *Eur. Biophys. J.* 34:359–368.
- Laver, D. R., L. D. Roden, G. P. Ahern, K. R. Eager, P. R. Junankar, and A. F. Dalhenty. 1995. Cytosolic Ca²⁺ inhibits the ryanodine receptor from cardiac muscle. *J. Membr. Biol.* 147:7–22.
- O'Neill, E. R., M. M. Sakowska, and D. R. Laver. 2003. Regulation of the calcium release channel from skeletal muscle by suramin and the disulfonated stilbene derivatives DIDS, DBDS, and DNDS. *Biophys. J.* 84:1674–1689.
- Marks, P. W., and F. R. Maxfield. 1991. Preparation of solutions with free calcium concentration in the nanomolar range using 1,2-bis(o-aminophenoxy)ethane-*n,n,n',n'*-tetraacetic acid. *Anal. Biochem.* 193: 61–71.
- Brooks, S. P., and K. B. Storey. 1992. Bound and determined: a computer program for making buffers of defined ion concentrations. *Anal. Biochem.* 201:119–126.
- Sigworth, F. J., and S. M. Sine. 1987. Data transformations for improved display and fitting of single-channel dwell time histograms. *Biophys. J.* 52:1047–1054.
- Chung, S. H., J. B. Moore, L. G. Xia, L. S. Premkumar, and P. W. Gage. 1990. Characterization of single channel currents using digital signal processing techniques based on Hidden Markov Models. *Philos. Trans. R. Soc. Lond. Biol.* 329:265–285.
- Zahradnikova, A., and I. Zahradnik. 1996. A minimal gating model for the cardiac calcium release channel. *Biophys. J.* 71:2996–3012.
- Zahradnik, I., S. Gyorke, and A. Zahradnikova. 2005. Calcium activation of ryanodine receptor channels—reconciling RyR gating models with tetrameric channel structure. *J. Gen. Physiol.* 126:515–527.
- Stern, M. D. 1992. Buffering of calcium in the vicinity of a channel pore. *Cell Calcium*. 13:183–192.
- Tinker, A., A. R. Lindsay, and A. J. Williams. 1992. A model for ionic conduction in the ryanodine receptor channel of sheep cardiac muscle sarcoplasmic reticulum. *J. Gen. Physiol.* 100:495–517.
- Lukyanenko, V., I. Gyorke, and S. Gyorke. 1996. Regulation of calcium release by calcium inside the sarcoplasmic reticulum in ventricular myocytes. *Pflugers Arch.* 432:1047–1054.
- Gyorke, I., and S. Gyorke. 1998. Regulation of the cardiac ryanodine receptor channel by luminal Ca²⁺ involves luminal Ca²⁺ sensing sites. *Biophys. J.* 75:2801–2810.
- McGarry, S. J., and A. J. Williams. 1994. Adenosine discriminates between the caffeine and adenine nucleotide sites on the sheep cardiac sarcoplasmic reticulum calcium-release channel. *J. Membr. Biol.* 137: 169–177.
- Protasi, F., C. Franzini-Armstrong, and B. E. Flucher. 1997. Coordinated incorporation of skeletal muscle dihydropyridine receptors and ryanodine receptors in peripheral couplings of BC3H1 cells. *J. Cell Biol.* 137:859–870.
- Somlyo, A. V., H. G. Gonzalez-Serratos, H. Shuman, G. McClellan, and A. P. Somlyo. 1981. Calcium release and ionic changes in the sarcoplasmic reticulum of tetanized muscle: an electron-probe study. *J. Cell Biol.* 90:577–594.
- Gyorke, S., and M. Fill. 1993. Ryanodine receptor adaptation: control mechanism of Ca²⁺-induced Ca²⁺ release in heart. *Science*. 260:807–809.
- Schiefer, A., G. Meissner, and G. Isenberg. 1995. Ca²⁺ activation and Ca²⁺ inactivation of canine reconstituted cardiac sarcoplasmic reticulum Ca²⁺-release channels. *J. Physiol. (Lond.)*. 289:337–348.
- Laver, D. R., T. M. Baynes, and A. F. Dulhunty. 1997. Magnesium inhibition of ryanodine-receptor calcium channels: evidence for two independent mechanisms. *J. Membr. Biol.* 156:213–229.
- Samsó, M., T. Wagenknecht, and P. D. Allen. 2005. Internal structure and visualization of transmembrane domains of the RyR1 calcium release channel by cryo-EM. *Nat. Struct. Mol. Biol.* 12:539–544.

37. Sitsapesan, R., and A. J. Williams. 1994. Gating of the native and purified cardiac SR Ca²⁺-release channels with monovalent cations as permeant species. *Biophys. J.* 67:1484–1494.
38. Sitsapesan, R., and A. J. Williams. 1990. Mechanisms of caffeine activation of single calcium-release channels of sheep cardiac sarcoplasmic reticulum. *J. Physiol. (Lond.)* 423:425–439.
39. Williams, A. J., and S. R. Holmberg. 1990. Sulmazole (AR-L 115BS) activates the sheep cardiac muscle sarcoplasmic reticulum calcium-release channel in the presence and absence of calcium. *J. Membr. Biol.* 115:167–178.
40. Smith, J. S., R. Coronado, and G. Meissner. 1986. Single channel measurements of the calcium release channel from skeletal muscle sarcoplasmic reticulum. Activation by Ca²⁺ and ATP and modulation by Mg²⁺. *J. Gen. Physiol.* 88:573–588.
41. Meissner, G. 1994. Ryanodine receptor/Ca²⁺ release channels and their regulation by endogenous effectors. *Annu. Rev. Physiol.* 56:485–508.
42. Meissner, G., and J. S. Henderson. 1987. Rapid calcium release from cardiac sarcoplasmic reticulum vesicles is dependent on Ca²⁺ and is modulated by Mg²⁺, adenine nucleotide, and calmodulin. *J. Biol. Chem.* 262:3065–3073.
43. Jiang, D., R. Wang, B. Xiao, H. Kong, D. J. Hunt, P. Choi, L. Zhang, and S. R. W. Chen. 2005. Enhanced store overload-induced Ca²⁺ release and channel sensitivity to luminal Ca²⁺ activation are common defects of RyR₂ mutations linked to ventricular tachycardia and sudden death. *Circ. Res.* 97:1173–1181.
44. Honen, B. N., D. A. Saint, and D. R. Laver. 2003. Suppression of calcium sparks in rat ventricular myocytes and direct inhibition of sheep cardiac RyR channels by EPA, DHA and oleic acid. *J. Membr. Biol.* 196:95–103.
45. Swan, J. S., K. Dibb, N. Negretti, S. C. O'Neill, and R. Sitsapesan. 2003. Effects of eicosapentaenoic acid on cardiac SR Ca²⁺-release and ryanodine receptor function. *Cardiovasc. Res.* 60:337–346.
46. Gyorke, I., N. Hester, L. R. Jones, and S. Gyorke. 2004. The role of calsequestrin, triadin, and junctin in conferring cardiac ryanodine receptor responsiveness to luminal calcium. *Biophys. J.* 86:2121–2128.
47. Xu, L., and G. Meissner. 2004. Mechanism of calmodulin inhibition of cardiac sarcoplasmic reticulum Ca²⁺ release channel (ryanodine receptor). *Biophys. J.* 86:797–804.
48. Lukyanenko, V., S. Viatchenko-Karpinski, A. Smirnov, T. F. Wiesner, and S. Gyorke. 2001. Dynamic regulation of sarcoplasmic reticulum Ca²⁺ content and release by luminal Ca²⁺-sensitive leak in rat ventricular myocytes. *Biophys. J.* 81:785–798.
49. Yang, Z., and D. S. Steele. 2001. Effects of cytosolic ATP on Ca²⁺ sparks and SR Ca²⁺ content in permeabilized cardiac myocytes. *Circ. Res.* 89:526–533.